JOURNAL OF AIRCRAFT
Vol. 34, No. 5, September–October 1997

New Computational Methods for the Prediction and Analysis of Helicopter Noise

Roger C. Strawn,* Leonid Oliker,† and Rupak Biswas‡
NASA Ames Research Center, Moffett Field, California 94035-1000

This paper describes a new methodology to predict and analyze rotorcraft noise. This methodology includes 1) a combined computational fluid dynamics and Kirchhoff scheme for far-field noise predictions, 2) parallel computer implementation of the Kirchhoff integrations, 3) audio and visual rendering of the computed acoustic predictions over large far-field regions, and 4) acoustic tracebacks to the Kirchhoff surface to pinpoint the sources of the rotor noise. This paper describes each method and presents sample results for three test cases. The first case consists of in-plane high-speed impulsive noise, and the other two cases show idealized parallel and oblique blade-vortex interactions. The computed results show good agreement with available experimental data, but convey much more information about the far-field noise propagation. When taken together, these analysis techniques exploit the power of new computer technologies and offer the potential to significantly improve our prediction and understanding of rotorcraft noise.

Introduction

FUTURE helicopter and tiltrotor designs must have low noise if they are to operate successfully near heavily populated areas. This requires the reduction of two main types of impulsive aerodynamic noise from the rotor system. The first is called high-speed impulsive (HSI) noise and is characterized by a strong acoustic disturbance that emanates from the rotor-blade tips. In this paper, we use the term HSI noise to represent the total acoustic signal that radiates from the rotor tips, including both the thickness and quadrupole terms in the Ffowcs Williams and Hawkings equation.[1] High-speed impulsive noise is generally a problem for helicopters rotors when their advancing-tip Mach numbers exceed 0.9.

The second type of impulsive noise comes from the interaction of the rotor blades with their vortical wake systems. These interactions cause rapid changes in blade airloads that lead to high noise in the far field. These blade-vortex interactions (BVIs) are particularly important near urban areas and are most prevalent when helicopters are descending for landings.

Rotorcraft designers require three things to systematically reduce HSI and BVI noise. First, they need high-accuracy methods for predicting far-field rotor noise. Second, they need a way to analyze these predictions that identifies the causes of the offending noise. The third requirement is an ability to alter the rotor blade shape or the rotor blade motion to reduce the far-field noise. This paper describes a new acoustics prediction and analysis methodology that addresses the first two of these three objectives. This new methodology focuses heavily on new and emerging computer algorithms, audio and visual rendering tools, and parallel processing. These new techniques provide a powerful framework for improved understanding of rotorcraft noise with an aim to reducing it.

Presented as Paper 96-1696 at the AIAA/CEAS 2nd Aeroacoustics Conference, State College, PA, May 6–8, 1996; received May 28, 1996; revision received April 25, 1997; accepted for publication April 28, 1997.

*Research Scientist, U.S. Army Aeroflightdynamics Directorate, M/S 258-1. Senior Member AIAA.

†Graduate Student, Department of Computer Science, University of Colorado, Boulder, CO; currently at Research Institute for Advanced Computer Science, M/S T27A-1.

‡Research Scientist; currently at MRJ Technology Solutions, M/S T27A-1.

Recent advances in rotorcraft noise prediction have come from combinations of computational fluid dynamics (CFD) and Kirchhoff methods. Finite difference solutions to the full potential or Euler/Navier–Stokes equations are used close to the rotor blades to model the near-field aerodynamics and acoustics. These near-field solutions are then interpolated onto a surface that completely encloses the rotor blades. A Kirchhoff integration over this surface carries the near-field acoustics solution to any point in the far field. These hybrid methods have the advantage that the nonlinear acoustic propagation is accurately modeled by the CFD solution close to the rotor blades where compressibility is important. Away from the rotor blades, it is no longer practical to compute the CFD solution over a large volume because numerical dissipation causes a loss of accuracy in the acoustic signal. The Kirchhoff integration is much more computationally efficient than the CFD methods for acoustic propagation over large distances with no dissipation. It assumes a constant speed of sound outside the Kirchhoff surface, which is a very good approximation away from the rotor blades. Examples of these hybrid CFD/Kirchhoff methods for computing both HSI and BVI helicopter noise are given in Refs. 2–12.

Up until now, these CFD/Kirchhoff techniques have been used to compute acoustic signals at a handful of far-field observer locations to compare with experimental microphone measurements. While these types of comparisons are useful for the purpose of validation, they do not exploit the full capabilities of these new acoustic prediction methods. The CFD/Kirchhoff formulations can compute far-field acoustic pressures at many observer locations covering large regions of the flowfield. When viewed as a whole, these acoustic signals give a great deal of insight into the far-field propagation characteristics of helicopter noise. This is particularly important for tiltrotor BVIs, where many of the noise generation and propagation mechanisms are not fully understood. Recent papers by Lowson[13] and Sim et al.[14] clearly emphasize the need for detailed studies of far-field helicopter noise propagation. Similar audio and visual analyses can be performed with acoustic analogy methods such as the Ffowcs Williams and Hawkings equation[1]; however, it is easier to include the effects of nonlinear acoustic propagation with the CFD/Kirchhoff method.

This paper describes several new computational tools for computing and analyzing helicopter noise in the far field using the new CFD/Kirchhoff formulation. First, we present a method for speeding up the Kirchhoff integrations so that sev-

eral thousand acoustic signals can be computed in a few hours. We accomplish this by running the Kirchhoff code on an IBM SP2 multiprocessor. The Kirchhoff integration is very well suited for parallel implementation and gives near-ideal speedups when modified to run on the SP2. Once the Kirchhoff code has computed the acoustic signals for all of the far-field observer locations, these signals are postprocessed to obtain visual and auditory information about the resulting noise. A computer graphics program creates animated three-dimensional images of the acoustic pressure waves; whereas an interactive audio system converts the computed digital acoustic signals into sound. In addition, we present a new technique to identify the sources of far-field noise on the Kirchhoff surface. We demonstrate these new analysis tools for rotorcraft cases with both HSI and BVI noise.

CFD/Kirchhoff Integration Method

The CFD/Kirchhoff method consists of a CFD solution near the rotor blades followed by a Kirchhoff integration to propagate the acoustic signals to the far field. In this paper, an Euler/Navier–Stokes flow solver called TURNS[15,16] computes the near-blade CFD solution. The TURNS code solves the Navier–Stokes equations about rotating helicopter blades. Since viscous effects are small for the cases considered in this paper, we run the TURNS code in the Euler mode. All nonlinear effects on the acoustic propagation are accurately modeled within the framework of the Euler equations.

The Kirchhoff formulation from Farassat and Myers[17] is used to evaluate the acoustic pressure P at a fixed observer location $\boldsymbol{x}$ and observer time t. In the general case, the Kirchhoff surface S can deform and have arbitrary motion; however, the applications in this paper use a nonrotational, rigid surface, with linear translational motion. With these simplifications, the Kirchhoff formula becomes

$$P(\boldsymbol{x}, t) = \frac{1}{4\pi} \int_S \left[\frac{E_1}{|\boldsymbol{r}|(1 - M_r)} + \frac{E_2 P}{r^2(1 - M_r)} \right]_\tau \mathrm{d}S \qquad (1)$$

The expressions for E_1 and E_2 are given as

$$E_1 = (M_n^2 - 1)P_n + M_n \boldsymbol{M}_t \cdot \nabla_2 P - \frac{M_n \dot{P}}{a_\infty} + \frac{(\cos\theta - M_n)\dot{P}}{a_\infty(1 - M_r)} \qquad (2)$$

$$E_2 = \frac{(1 - M^2)(\cos\theta - M_n)}{(1 - M_r)^2} \qquad (3)$$

The Kirchhoff surface translates with the rotor hub at Mach number $\boldsymbol{M}$. The distance between a point on the Kirchhoff surface and the observer is given by $|\boldsymbol{r}|$. M_n and M_r are the components of $\boldsymbol{M}$ along the local surface normal $\boldsymbol{n}$ and the radiation direction $\boldsymbol{r}$. $\boldsymbol{M}_t$ is the Mach number tangent to the Kirchhoff surface, P_n is the derivative of P along the surface normal, $\dot{P}$ is the time derivative of pressure, and $\nabla_2 P$ is the gradient of the pressure on the Kirchhoff surface. The freestream speed of sound is assumed uniform at a_∞, and θ is the angle between $\boldsymbol{n}$ and $\boldsymbol{r}$. The simplified form for E_2 in Eq. (3) is taken from Myers and Hausmann.[18] The observer can either be moving or stationary. An observer that moves with the rotor hub corresponds to a wind-tunnel noise simulation, and a stationary observer represents a helicopter flyover.

Figure 1 shows a representative Kirchhoff surface in the nonrotating reference frame. The rotor blades spin inside the surface that consists of top, bottom, and side meshes. Each of these three meshes is discretized with approximately 30,000 points. Evaluation of the acoustic pressure in Eq. (1) first requires a spatial interpolation of pressure and pressure derivatives from the rotating CFD grid onto the nonrotating Kirchhoff mesh. These spatial interpolations are performed in the CFD code at run time. The interpolated Kirchhoff surface pressures and pressure derivatives are written to disk at typical

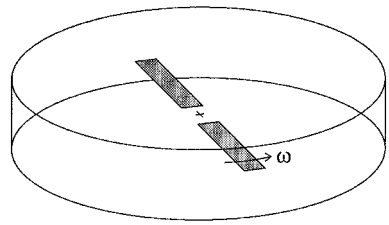

Fig. 1 Helicopter blades rotate inside the nonrotating Kirchhoff surface.

intervals of a 1-deg azimuthal angle for a complete cycle of blade rotation. Overset grid techniques are used for the spatial interpolations onto the Kirchhoff surface. Either the DCF3D code from Meakin,[19] or the PEGSUS code from Suhs and Tramel[20] can be used for these interpolations with a negligible impact on run time for the CFD codes. References 8 and 12 give details on these interpolation techniques; Refs. 7 and 8 provide additional details on the Kirchhoff formulation.

Evaluation of the acoustic pressure in Eqs. (1)–(3) also requires a temporal interpolation in the stored database of Kirchhoff-surface pressures. The integrand must be evaluated at the time of emission τ for each differential area on the Kirchhoff surface. This is also known as the retarded time. Appropriate values of retarded time are determined by noting that the time delay between the emission of the acoustic signal and its arrival at the observer is equal to the distance that this signal must travel, divided by the freestream speed of sound. This formulation leads to a quadratic equation for τ. One of the roots is nonphysical and discarded. We retrieve the appropriate pressure and pressure derivatives at this emission time using linear temporal interpolation in the database of stored pressure values on the Kirchhoff surface.

For a Kirchhoff surface with 86,400 points, the Kirchhoff integration code requires 0.05 Cray C-90 CPU seconds for each pressure evaluation in Eqs. (1)–(3), at an observer location $\boldsymbol{x}$ in space, and an observer time t. Thus, at each observer location, these numbers correspond to a total of 9 Cray C-90 CPU seconds for a periodic time–history consisting of 180 pressure evaluations. The Kirchhoff program runs at 470 MFLOPS on the C-90. Improved coding for the temporal interpolations gives an overall speed that is approximately 20 times faster than the CPU times reported in Ref. 8.

An alternative to the nonrotating Kirchhoff formulation described earlier is to use a Kirchhoff surface that rotates with the rotor blades. The advantage of this rotating-surface formulation is that spatial interpolations onto the Kirchhoff surface are not required since the Kirchhoff grid coincides with part of the rotating CFD mesh. Also, the rotating Kirchhoff surface typically requires fewer grid points than a nonrotating one. Reference 8 presents results from both the rotating- and the nonrotating-surface Kirchhoff methods. The two methods used the same CFD solutions as inputs and gave similar results. Computer resource requirements were comparable for both methods; however, the nonrotating-surface method was more robust, particularly for high-speed rotor cases.

One potential problem with the Kirchhoff formulation is that it contains a Doppler singularity that requires subsonic motion of the Kirchhoff surface. This requirement places a restriction on the outer radial location for a rotating Kirchhoff surface. If it is too far from the rotor blade tip, it will have supersonic motion, which is not allowed. On the other hand, if the surface is too close, then the acoustic solution may be inaccurate. The nonrotating-surface formulation removes the rotational component of motion from the Kirchhoff surface. The resulting translational motion is always subsonic for a helicopter rotor. Thus, the nonrotating Kirchhoff formulation avoids the Doppler singularity problem.

Parallel Implementation

Implementation of the rotating and nonrotating Kirchhoff integrations on parallel computers is straightforward because the Kirchhoff-surface is composed of regular structured grids that require very little processor-to-processor communication during the computation. The Kirchhoff surface is divided into patches, and each patch is assigned to a processor. Virtually no communication is needed among processors except for the final summation of the integral contributions from each surface patch. The Kirchhoff integrations were run on the 148-node IBM SP2 multiprocessor installed at NASA Ames Research Center. The parallel code uses a message-passing paradigm and is portable to any distributed-memory architecture that supports Fortran 90 and the MPI (message-passing interface) library.

The Kirchhoff surface and associated pressure files are stored as a series of two-dimensional arrays, each with a size of $(i_{\max}, j_{\max})$. These data must be partitioned and distributed among the processors to run the computation. Since our SP2 is restricted to serial I/O, one host processor reads and scatters the data to the working set of P processors. Each processor receives a contiguous strip of $(i_{\max} \times j_{\max})/P$ rectangular elements of the Kirchhoff surface. Each rectangular element on the Kirchhoff surface is composed of four node points and associated pressure data. This partitioning provides for balanced loads among the processors and local nearest-neighbor computations on each processor, thereby minimizing cache memory misses.

A more memory-efficient way to partition the Kirchhoff surface data to the processors would be to use two-dimensional blocks of $(i_{\max}/P, j_{\max}/P)$ surface elements on each processor. This strategy would significantly reduce the required data overlap at the nodal boundaries between partitions. However, this two-dimensional partitioning of surface elements would degrade the cache performance on each processor and complicate the local index computations when compared to the one-dimensional surface-element partitioning described earlier. Because of the relatively small value of $i_{\max}$ compared to the available memory on each processor, we chose the one-dimensional partitioning so that each processor receives contiguous strips of surface elements.

Another possible parallel strategy for this problem is to split the far-field observer locations equally among the processors. This implementation would be the most memory-intensive of any approach, since each processor would require a local copy of the entire database of Kirchhoff-surface pressure information. However, computational time would be similar to that required by the other partitioning strategies.

Because no communication is required until a final global summation, and the I/O is independent of the number of processors, the actual run time on the SP2 scales by over 98% as the number of processors increases. As a result, with 60 processors on the SP2, and 86,400 points on the Kirchhoff surface, we can compute a periodic time history of 180 pressure evaluations for each of 7533 far-field observer locations in about five CPU hours. A similar calculation on one processor of a Cray C-90 requires over 20 CPU hours. The real payoff, however, comes from the scalability of the parallel implementation. This same calculation would require only about 35 CPU minutes to complete on a 512-node SP2.

Visual Postprocessing

Figure 2 shows a sample grid of far-field observer locations for the operational loads survey (OLS) rotor that was experimentally tested by Schmitz et al.[21] These grid points are located in the plane of the rotor between 2–12 blade radii from the rotor hub. Overall, this grid contains a total of 7533 observer points. Time histories of acoustic pressure were computed for each of these observer locations using the parallel Kirchhoff code on an SP2. These unsteady results were then animated and visualized on a Silicon Graphics workstation.

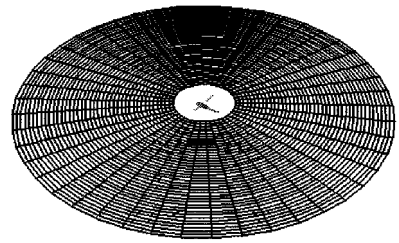

Fig. 2 Far-field grid of observer points for the Kirchhoff acoustics simulation.

The animated results give a clear picture of the unsteady propagation of acoustic signals in the far field, as will be shown later in this paper. This approach has the advantage that the entire field can be viewed at once. It conveys much more information than what can be seen from a handful of far-field experimental microphones. Another benefit of the Kirchhoff animations is that they can cover large regions of the acoustic far field with high accuracy. Wind-tunnel geometric constraints typically limit experimental microphone placement to a region that is less than three or four radii from the rotor blades. These microphone locations may be too close to accurately represent the acoustic far-field propagation. There is no restriction, however, on the locations of the far-field observer points in the computer simulations.

Audio Postprocessing

Time-dependent CFD/Kirchhoff rotorcraft acoustic simulations are well-suited for audio playback. The CFD/Kirchhoff integration provides pressure data at discrete locations in the far-field, such as those shown in Fig. 2. Audio playback is obtained by using the Stereophonic Acoustics Software Library that has been recently developed at NASA Ames Research Center. This software package allows the user to interactively select individual grid points where pressure data can be played over headphones or stereo speakers connected to a Silicon Graphics Indigo computer. The digital pressures for the entire field are scanned for maximum and minimum amplitudes and then scaled for 16-bit stereo sound. The user can add a slight phase shift between the signals for each ear for added realism. This phase shift simulates the interaural time delay that conveys spatialized acoustic perceptions to the human brain.

Sample computed results for the OLS rotor cases in Ref. 21 have been processed for the audio playback described earlier. Although we cannot effectively convey the audio results in this paper, they are quite realistic. This is particularly true when played back on audio systems with powerful amplifiers and accurate low-frequency response.

Identification of Noise Sources

The successful design of low-noise rotors requires a connection between far-field noise predictions and the sources of noise at the rotor disk. This is particularly true for BVI cases where the highest noise levels may originate from only one or two localized BVIs. A relatively small change in blade trajectory and/or blade geometry may locally increase the miss distance for a BVI event and drastically reduce the far-field noise. The main design issues are where and how to modify the blade shapes and/or blade motions to control these BVIs.

The nonrotating Kirchhoff formulation can be modified to provide information on the locations of the main sources of rotor noise. We accomplish this by computing the integrand in Eq. (1) at each node on the Kirchhoff surface at a particular observer location and time when the noise level is high. Recall that these integrands are all evaluated at different retarded times. A contour plot is then constructed from these nodal integrand values. This contour plot shows the relative contri-

butions from each surface point to the far-field acoustic pressure. Such a plot is similar to a source strength distribution on an acoustic planform; however, the shape of the Kirchhoff surface does not change with time.

Although these Kirchhoff-surface contour plots represent noise that originates at the rotor blades, the precise locations of the rotor blades are still in question at the time when this noise was produced. This uncertainty arises from the finite propagation distance between the rotor blades to the Kirchhoff surface. However, this propagation distance is small since the Kirchhoff surface is only one or two chords away from the rotor disk. Thus, the locations of high noise contributions at the Kirchhoff surface should roughly correspond to the locations of the rotor blades when these noise contributions were produced.

When paired with some knowledge of the rotor tip–vortex locations, a designer can identify the rotor BVI events that produce the far-field noise. Modification of the blade trajectories and/or tip–vortex production in these regions has a high potential for noise reduction in the far field. We use the term, Kirchhoff-surface acoustic tracebacks, to describe this noise-source identification technique. It was first used in Ref. 12 for cases with HSI noise. Applications of the technique for BVI noise are described later in this paper.

Results: High-Speed Impulsive Noise

The acoustic analysis methods described earlier have been applied to the OLS rotor blade cases that were experimentally tested by Schmitz et al.[21] In this experiment, acoustic signals were recorded at several far-field locations from a 1/7 scale model of the Army's AH-1 two-bladed helicopter main rotor. The test condition for this paper has a hover-tip Mach number of 0.665 and an advance ratio of 0.258. This yields a maximum advancing-tip Mach number of 0.837 and significant transonic flow on the advancing side of the rotor disk. This case is modeled as a nonlifting rotor blade to simplify the CFD analysis. Lifting rotor calculations require fine grids to capture the rotor wake systems. This is not necessary in this case since rotor lift has little effect on HSI noise in the plane of the rotor blades.[21] The Kirchhoff surface is located approximately 1.5 chords from the rotor blade in all directions.

Reference 8 describes this case in more detail and gives comparisons of predicted acoustic pressures using the CFD/Kirchhoff method to the experimental microphone data at several locations in the far field. Figure 3 shows one of these comparisons for a microphone located in the plane of the rotor and 3.44 rotor radii directly upwind from the rotor hub. The comparison shows good agreement between the prediction and the experimental data. Reference 8 shows similar results for the other microphone locations.

The observer grid in Fig. 2 is used for computing the far-field acoustic pressures in the plane of the rotor blades. A relatively fine (81 × 93) grid of far-field observers is used since the propagating acoustic waves are highly impulsive. The use of coarse grids causes interpolation errors when the acoustic waves are not aligned with the far-field observer grid. The TURNS code for this case required approximately 2.5 C-90 CPU hours to complete the unsteady solution for one blade revolution on a 135 × 50 × 35 grid. The CPU requirement for interpolations onto the Kirchhoff surface is negligible. The nonrotating Kirchhoff surface consists of 86,400 mesh points and the temporal resolution for the observer locations corresponds to 1 deg of blade azimuthal angle. This means that 180 Kirchhoff integrations are required at each of 7533 observer locations to obtain the predictions for one rotor cycle.

Figure 4 shows a photograph from an animation of the far-field acoustic pressure contours. The time corresponds to rotor blade positions of 90- and 270-deg azimuthal angle. These pressure values are scaled by the distance from the rotor hub, which helps to show the directivity of the noise in the far field. The highest-scaled acoustic amplitude occurs along the direction of flight, directly ahead of the rotor blade and slightly to the advancing side. The experimental data[21] also show this same behavior.

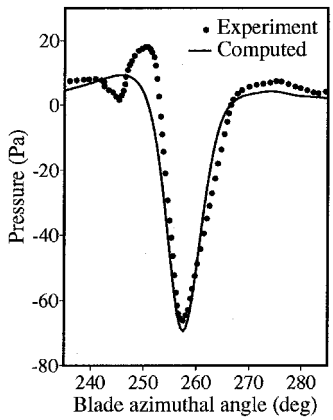

Fig. 3 Comparison of predicted and experimental acoustic pressure data for the OLS rotor blade.

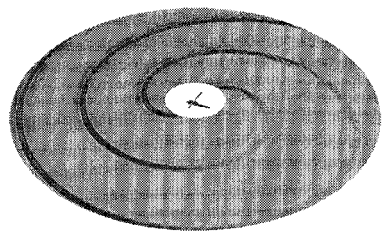

Fig. 4 Acoustic pressures in the plane of the rotor for the OLS rotor blade.

The animated results give a clear picture of the unsteady propagation of acoustic signals in the far field. The advantage of this approach is that the entire field can be viewed at once. This global view conveys much more information than that obtained from a handful of experimental microphones, an important consideration when evaluating different rotor designs for far-field noise reduction. With a limited number of experimental microphones, one runs the risk that a design change may locally reduce the noise at a single microphone, but increase the noise in a region where no microphones are present. In addition to providing a global view of the far-field noise, the CFD/Kirchhoff calculations also provide acoustic information at much larger distances from the rotor hub than wind-tunnel experiments.

The time-dependent CFD/Kirchhoff results in Fig. 4 are well-suited for audio playback. The acoustic predictions have been incorporated into an interactive computer simulation that allows the user to choose any position in the far-field relative to the spinning rotor system. The computer screen shows the helicopter fuselage and spinning rotor blades from this viewpoint. Once the viewpoint is set, the simulation reads from the stored far-field acoustic pressures to produce an audio rendering of the helicopter noise. The viewpoint can be changed to allow the user to compare the rotor noise at different locations. This type of simulation is a good model for a virtual environment that allows for rapid comparisons of helicopter noise in urban environments with a variety of flight paths for approach and landing.

Parallel BVI Noise

We have also used the new acoustics analysis techniques to simulate the isolated parallel BVI experiment of Kitaplioglu and Caradonna.[22] In the experiment, a vortex generator is placed upstream of a rotor in a wind tunnel. The vortex generator produces a vortex of known strength and trajectory. This vortex interacts with the rotor blades to produce rapid changes in lift that characterize the BVI event. The rectangular rotor has a radius of 7.125 blade chords and a NACA 0012 airfoil section. Figure 5 shows a schematic of the experimental and

computational setup. As shown in Fig. 5, an experimental microphone array is located 20 chords from the rotor hub at the 270-deg azimuthal angle position on the retreating side of the rotor disk. Positive azimuthal angles are defined in the counterclockwise direction, with 0 deg being farthest away from the oncoming freestream velocity.

The computed test case is the same as that given in Ref. 8. The TURNS code models the vortex analytically as described in Refs. 23 and 24 and computes the surrounding flowfield to satisfy the conservation equations. The analytic vortex model simplifies the analysis since the vortex cannot diffuse from numerical dissipation in the CFD method. The rotor blade is set at zero angle of attack, which means that the lift forces on the blade arise only from the BVIs. Computation times and grid sizes for this BVI case are essentially the same as those for the HSI case described earlier. Numerical experiments showed that time steps equal to 0.25 deg of a rotor azimuthal angle with three Newton subiterations per time step give far-field noise results that are independent of the grid size and choice of time step.

The test case has a hover-tip Mach number of 0.713 and an advance ratio of 0.197. The vortex has a strength of $1.05V_\infty c$, where V_∞ is the tunnel freestream velocity and c is the rotor chord. The sign of the vorticity is opposite to the direction of the freestream velocity, and the vortex passes through the rotor hub one-quarter chord below the rotor disk. The Kirchhoff surface for this case is approximately 1.5 chords away from the rotor blades in all directions, and numerical studies in Ref. 8 indicate that the computed noise is grid-independent at this Kirchhoff-surface location.

Figure 6 compares computed and experimental pressure values for two microphone locations. Microphones 2 and 5 are located 12.49 and 21.45 chords below the plane of the rotor, respectively. Additional comparisons between computations and experiments are presented in Ref. 8. The computations and experimental data show excellent agreement for the positive part of the BVI signal. However, the computations also show a negative signal that is not present in the experimental data.

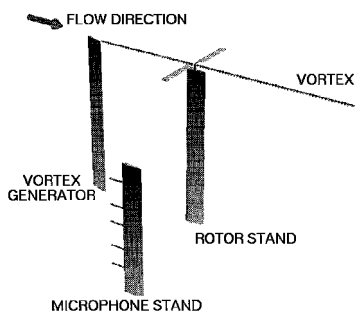

Fig. 5 Experimental and computational setup for the parallel BVI.

Three different planar observer meshes were used to animate the resulting far-field noise propagation. Each mesh contained 7533 points and covered a region extending from 2 to 12 blade radii similar to that shown in Fig. 2. One of the meshes is located in the plane of the rotor blades, and the other two are 21.45 and 10.725 chords below the rotor plane.

Figure 7 shows a close-up of the acoustic pressure contours 21.45 chords below the rotor disk near the experimental microphone stand. Three separate acoustic waves are visible in this figure. First, the far-left side of the figure shows a wave that propagates upstream from the rotor hub. Although it is not visible from the grayscale image in Fig. 7, analysis of color contours shows that this wave has negative acoustic pressure and originates on the advancing side of the rotor disk near a blade azimuthal angle of 90 deg. The CFD calculation shows quite a bit of transonic flow in this region, and the resulting acoustic signal propagates ahead of the rotor as HSI noise.

The other two pressure waves are circular with their centers offset by approximately one rotor diameter. The circular wave on the left has a positive pressure and is produced by the BVI when the blade is located at 180-deg azimuthal angle. The second wave has a negative pressure and results from the BVI at 0-deg azimuthal angle. The BVI acoustic waves generally propagate in a dipole pattern,[25] which explains why they intersect the observer plane in a circle.

Note that the two circular BVI waves intersect near the location of the experimental microphones on the retreating side of the rotor disk. The negative wave from the 0-deg BVI passes over the microphones slightly behind the positive wave from the 180-deg BVI. This effect is reflected in Fig. 6, where the computed microphone pressure shows a positive peak, (a), followed by a negative peak, (b). Most likely, the vortex in the experiment dissipates considerably when it hits the rotor hub, and the BVI at the 0-deg location is not nearly as strong as the one at 180 deg. The computations assume that the vortex strength and core-size are undisturbed as it passes through the rotor hub, and that the vortices are identical at the 0- and 180-deg BVI locations. This assumption of constant vortex strength in the prediction explains the discrepancies between experimental and computational results in Fig. 6.

We can confirm this explanation by performing tracebacks to identify the sources of noise on the nonrotating Kirchhoff surface. The contributions from the Kirchhoff surface to the acoustic pressure peaks, (a) and (b), are shown in Fig. 8. The highest pressure contours in Fig. 8a are located near the 180-deg BVI location. The lowest pressure contours in Fig. 8b are located near the 0-deg BVI location. The resulting predicted acoustic pressures at microphone 5 show contributions from both of these BVI events. This case illustrates why it is important to include the contributions from all of the rotor blades when simulating general rotor BVI cases.

Figure 9 shows a far-field view of the propagating acoustic waves in the same plane as shown in Fig. 7. The two BVI waves propagate to the retreating and advancing sides of the

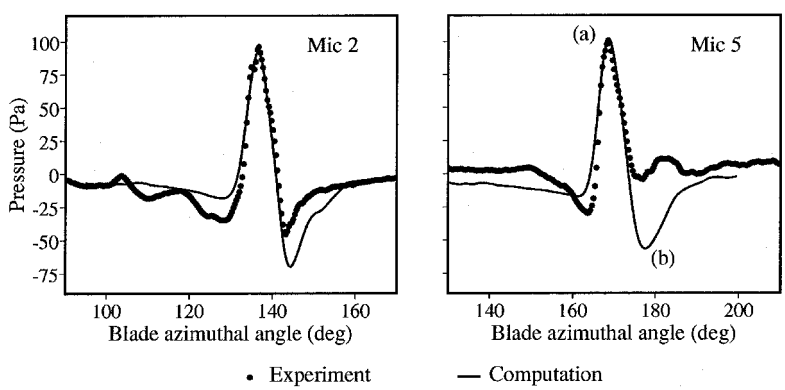

Fig. 6 Parallel BVI comparison of computed and experimental acoustic pressures.

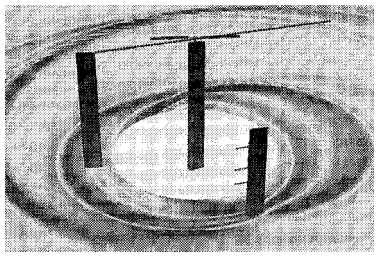

Fig. 7 Close-up of acoustic propagation for a parallel BVI at 21.45 chords below the rotor disk.

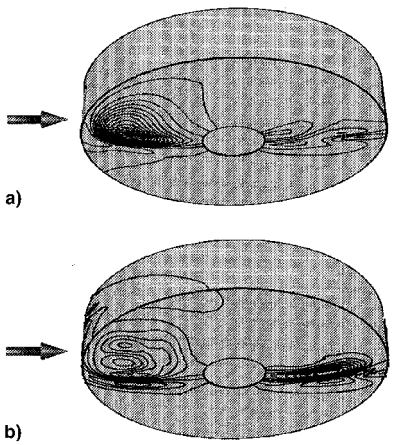

Fig. 8 Acoustic tracebacks on the Kirchhoff surface for the computed positive, (a), and negative, (b), pressure peaks at microphone 5. These views show the side and the bottom of the Kirchhoff surface.

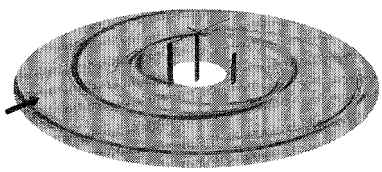

Fig. 9 Far-field view of parallel BVI acoustic propagation 21.45 chords below the rotor disk.

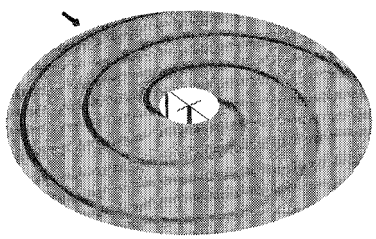

Fig. 10 Parallel BVI acoustic propagation in the plane of the rotor blades.

rotor disk while the HSI wave propagates upstream and dominates the acoustic signal in the far-field. It is clear from this figure that the computational results give a much more complete picture of the acoustic far field than the experimental data.

Figure 10 shows a photograph of the computed parallel BVI acoustic pressures in the plane of the rotor. Since the BVI acoustic waves propagate in dipole patterns, they are not visible here. HSI waves typically propagate in a monopole pattern[25] and these dominate the in-plane rotor noise. The highest amplitude acoustic signals propagate upstream from the rotor hub. All far-field acoustic pressure contours in this paper are scaled by the distance from the rotor hub.

Oblique BVI Noise

In addition to parallel BVIs, a more common scenario occurs when the vortex passes beneath the rotor blades at an oblique angle. We can simulate an idealized oblique interaction by moving the vortex generator away from the centerline of the rotor hub. Figure 11 shows such a case where the vortex has moved 2.13 chords toward the advancing side of the rotor disk. Caradonna et al.[26] tested this configuration in the U.S. Army Aeroflightdynamics Directorate 7 × 10-ft wind tunnel at NASA Ames Research Center, and recorded unsteady blade surface pressures. Far-field acoustic measurements were not recorded, however. Numerical simulations of this idealized oblique BVI were reported in Ref. 26 with a full-potential CFD code, and in Ref. 27 with an early version of the TURNS code.

The test conditions for this case have a hover-tip Mach number of 0.763 and an advance ratio of 0.197. The vortex has a strength of $1.218V_{\infty}c$, and the sign of the vorticity is aligned with the freestream velocity. The vortex is located 0.25 chords below the plane of the rotor, and the outer tip of the rotor blade passes over the vortex on the advancing side at 17- and at 163-deg blade azimuthal angles. Large regions of transonic flow occur near the tips of the rotor blades between 70- and 170-deg azimuthal angles. This means that the BVI event in the second quadrant of rotor motion is highly nonlinear and unsteady.

The TURNS code was run in the Euler mode for this simulation using the same computational grid that was used for the parallel interaction case. Because of the highly unsteady flow in the second quadrant of rotor motion, the time step was reduced to an equivalent of 0.125-deg azimuthal angle with five Newton subiterations at each time step. Numerical experiments showed that these choices yielded solutions that were independent of the choice of time step. Because of the strong transonic flow in this case, the Kirchhoff surface was located a distance of two chords from the rotor blades in all directions.

Computed results for blade surface pressures are similar to those computed by Caradonna et al.[26] and Srinivasan and McCroskey[27] for the same test case. Minor differences appear near the 165-deg azimuthal angle, where the highest transonic and unsteady effects are present. Differences between Ref. 27 and the current calculations are most likely because of the differences in the computational grids. Srinivasan and McCroskey[27] used a 21 × 101 × 15 O–O mesh with the outer boundaries located 8 chords from the rotor in all directions.

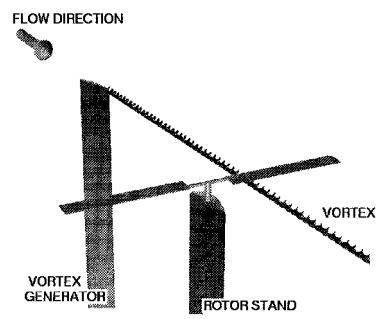

Fig. 11 Experimental and computational setup for an idealized oblique BVI.

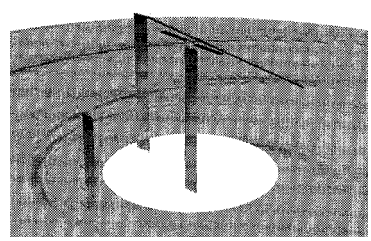

Fig. 12 Acoustic propagation for the oblique BVI.

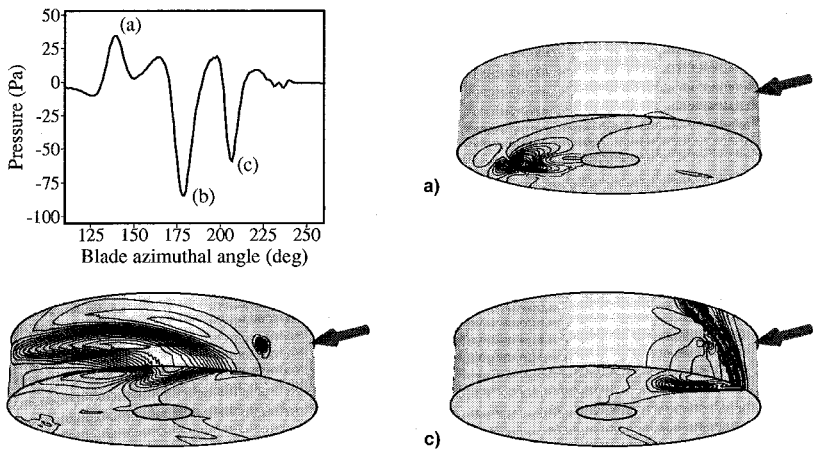

Fig. 13 Acoustic tracebacks on the Kirchhoff surface for an oblique BVI. The observer location is 30.28 chords upstream of the rotor hub and 21.45 chords below the plane of the rotor. Viewpoint shows bottom and side of the Kirchhoff surfaces.

The present calculations used a 151 × 40 × 50 C–H mesh with the outer boundaries located approximately 12 chords away from the rotor blade in all directions.

Figure 12 shows a photograph of the computed pressure contours in a plane 21.45 chords below the rotor disk. Three distinct acoustic waves can be seen in a region that is between 3–7 rotor radii upstream of the rotor hub. All three of these waves propagate upstream and each is caused by a different event on the rotor blades. The first of these three waves (as seen by a stationary observer) has a positive pressure and is the result of the downstream BVI event near the 17-deg blade azimuthal angle. The second wave has a negative pressure and is caused by the high-speed impulsive noise that emanates from the rotor blade tip in the second quadrant of rotor motion. The third wave also has a negative pressure and comes from the BVI event near the 163-deg blade azimuthal angle. The origins of these three acoustic waves are fairly clear from the complete color animation of the computed acoustic pressures. These noise sources can be confirmed by examining the acoustic tracebacks to the Kirchhoff surface for an observer that is located upstream of the rotor hub.

Figure 13 shows three acoustic tracebacks for an observer who is located 30.28 chords upstream from the rotor hub and 21.45 chords below the rotor disk. The pressure vs azimuthal angle plot shows that the observer hears three distinct pressure peaks, and these are labeled (a), (b), and (c) in Fig. 13. The first is a positive pressure, and the source of this noise is shown on the Kirchhoff surface in Fig. 13a. The main contribution to the pressure at point (a) comes from the lower part of the Kirchhoff surface, near the BVI event at the 17-deg blade azimuthal angle. The second pressure peak occurs at point (b), and almost all of the contributions here come from the advancing side of the Kirchhoff surface as shown in Fig. 13b. This negative pressure region is caused by HSI noise on the advancing side, which radiates from the rotor blades in a monopole pattern. Finally, the third pressure peak occurs at point (c), and the sources of this noise are shown in Fig. 13c. This figure shows both positive and negative pressures on the side of the Kirchhoff surface in the second quadrant. These disturbances result from the delocalized shock wave and their net contribution to the far-field observer pressure is small. The dominant contribution in Fig. 13c to the pressure peak at point (c) comes from the lower section of the Kirchhoff surface close to the BVI event near the 163-deg blade azimuthal angle. The acoustic tracebacks confirm the earlier explanation for the origins of the three acoustic waves shown in Fig. 12.

Summary and Conclusions

This paper describes a new methodology to predict and analyze rotorcraft noise. This methodology consists of 1) CFD/Kirchhoff far-field noise predictions, 2) parallel computer implementation of the Kirchhoff integrations, 3) audio and visual rendering of the computed acoustic predictions over large far-field regions, and 4) acoustic tracebacks to the Kirchhoff surface to pinpoint the sources of the rotor noise. When taken together, these techniques exploit the power of new computer technologies and offer the potential to significantly improve our prediction capabilities and understanding of rotorcraft noise.

These four prediction and analysis methods convey much more information about the propagation of rotorcraft noise than can be obtained from typical experiments. The visual rendering shows details of the acoustic propagation over large regions in the far field, and the acoustic tracebacks to the Kirchhoff surface help to identify the noise sources at the rotor disk. The computed results give an accurate picture of both the far-field noise and its origins on the rotor blades. The excellent parallel efficiency of the Kirchhoff integrations should allow for future acoustic simulations with larger numbers of far-field observers, possibly leading to fully three-dimensional animations of rotary–wing acoustic waves.

The current CFD/Kirchhoff methods provide accurate simulations for just about any type of in-plane HSI noise. This is because the rotor wake system does not play a major role in this type of noise. The CFD/Kirchhoff analysis would be a good candidate for a blade-design optimization study to reduce HSI noise. General cases with BVI noise are more difficult because the CFD codes must capture the rotor vortex wake systems without excessive numerical dissipation. The Kirchhoff integration method in this paper is compatible with any rotary–wing CFD code, so that future improvements in CFD wake capturing should directly result in improved BVI noise predictions.

Acknowledgments

The authors would like to thank Vee Hirsch for her work to produce a computer-animated video of the computations described in this paper. We would also like to thank G. R. Srinivasan for his help with the TURNS code for the oblique BVI case. Both of these individuals work for Sterling Software at NASA Ames Research Center.

References

[1]Ffowcs Williams, J. E., and Hawkings, D. L., "Sounds Generated by Turbulence and Surfaces in Arbitrary Motion," *Philosophical Transactions of the Royal Society of London, Series A: Mathematical and Physical Sciences*, Vol. 264, No. 1151, 1969, pp. 321–342.

[2]Xue, Y., and Lyrintzis, A. S., "Rotating Kirchhoff Method for Three-Dimensional Transonic Blade-Vortex Interaction Hover Noise," *AIAA Journal*, Vol. 32, No. 7, 1994, pp. 1350–1359.

[3]Lyrintzis, A. S., Kilaras, M. S., and Xue, Y., "Transonic 3-D BVI Noise Using a Rotating Kirchhoff Formulation for Advancing Rotors," *Proceedings of the 50th American Helicopter Society Annual Forum* (Washington, DC), 1994, pp. 115–127.

[4]Baeder, J. D., Gallman, J. M., and Yu, Y. H., "A Computational Study of the Aeroacoustics of Rotors in Hover," *Proceedings of the 49th American Helicopter Society Annual Forum* (St. Louis, MO), 1993, pp. 55–72.

[5]Strawn, R. C., Biswas, R., and Garceau, M., "Unstructured Adaptive Mesh Computations of Rotorcraft High-Speed Impulsive Noise," *Journal of Aircraft*, Vol. 32, No. 4, 1995, pp. 754–760.

[6]Strawn, R. C., and Biswas, R., "Numerical Simulations of Helicopter Aerodynamics and Acoustics," *Journal of Computational and Applied Mathematics*, Vol. 66, Nos. 1/2, 1996, pp. 471–483.

[7]Strawn, R. C., and Biswas, R., "Computation of Helicopter Rotor Noise in Forward Flight," *Journal of the American Helicopter Society*, Vol. 40, No. 3, 1995, pp. 66–72.

[8]Strawn, R. C., Biswas, R., and Lyrintzis, A. S., "Helicopter Noise Predictions Using Kirchhoff Methods," *Journal of Computational Acoustics*, Vol. 4, No. 3, 1996, pp. 321–339.

[9]Lyrintzis, A. S., "Review: The Use of Kirchhoff's Method in Computational Aeroacoustics," *Journal of Fluids Engineering*, Vol. 116, No. 4, 1994, pp. 665–675.

[10]Polacsek, C., and Costes, M., "Rotor Aeroacoustics at High-Speed Forward Flight Using a Coupled Full Potential/Kirchhoff Method," 21st European Rotorcraft Forum, Paper 1-5, St. Petersburg, Russia, Aug. 1995.

[11]Lyrintzis, A. S., Koutsavdis, E. K., Berizin, C. R., Visintainer, J. A., and Pollack, M. J., "Kirchhoff Acoustic Methodology Validation and Implementation in the Tiltrotor Aeroacoustic Codes (TRAC)," 2nd American Helicopter Society Aeromechanics Specialists' Conf., Paper 3-4, Bridgeport, CT, Oct. 1995.

[12]Duque, E. P. N., Strawn, R. C., Ahmad, J., and Biswas, R., "An Overset Grid Navier-Stokes/Kirchhoff-Surface Method for Rotorcraft Aeroacoustic Predictions," AIAA Paper 96-0152, Jan. 1996.

[13]Lowson, M., "Directionality of Helicopter BVI Noise," 21st European Rotorcraft Forum, Paper 3-5, St. Petersburg, Russia, Aug. 1995.

[14]Sim, B. W.-C., George, A. R., and Yen, S. J., "Blade-Vortex Interaction Directivity Studies Using Trace Mach Number," 2nd American Helicopter Society Aeromechanics Specialists' Conf., Paper 3-5, Bridgeport, CT, Oct. 1995.

[15]Srinivasan, G. R., Baeder, J. D., Obayashi, S., and McCroskey, W. J., "Flowfield of a Lifting Rotor in Hover: A Navier-Stokes Simulation," *AIAA Journal*, Vol. 30, No. 10, 1992, pp. 2371–2378.

[16]Srinivasan, G. R., and Baeder, J. D., "TURNS: A Free-Wake Euler/Navier-Stokes Numerical Method for Helicopter Rotors," *AIAA Journal*, Vol. 31, No. 5, 1993, pp. 959–962.

[17]Farassat, F., and Myers, M. K., "Extension of Kirchhoff's Formula to Radiation from Moving Surfaces," *Journal of Sound and Vibration*, Vol. 123, No. 3, 1988, pp. 451–460.

[18]Myers, M. K., and Hausmann, J. S., "On the Application of the Kirchhoff Formula for Moving Surfaces," *Journal of Sound and Vibration*, Vol. 139, No. 1, 1990, pp. 174–178.

[19]Meakin, R., "Moving-Body Overset Grid Methods for Complete Aircraft Tiltrotor Simulations," AIAA Paper 93-3350, July 1993.

[20]Suhs, N. E., and Tramel, R. E., "PEGSUS 4.0 Users Manual," Arnold Engineering Development Center, TR-91-8, June 1991.

[21]Schmitz, F. H., Boxwell, D. A., Splettstoesser, W. R., and Schultz, K. J., "Model-Rotor High-Speed Impulsive Noise: Full-Scale Comparisons and Parametric Variations," *Vertica*, Vol. 8, No. 4, 1984, pp. 395–422.

[22]Kitaplioglu, C., and Caradonna, F. X., "A Study of Blade-Vortex Interaction Aeroacoustics Utilizing an Independently-Generated Vortex," AGARD Fluid Dynamics Panel Symposium on Aerodynamics and Aeroacoustics of Rotorcraft, Paper 20, Berlin, Germany, Oct. 1994.

[23]Srinivasan, G. R., "A Free-Wake Euler and Navier-Stokes CFD Method and Its Application to Helicopter Rotors Including Dynamic Stall," JAI Associates, Inc., TR 93-01, Mt. View, CA, Nov. 1993.

[24]Baeder, J. D., and Srinivasan, G. R., "Computational Aeroacoustic Study of Blade-Vortex Interaction Noise," American Helicopter Society Aeromechanics Specialists' Meeting, Paper 1-5, San Francisco, CA, Jan. 1994.

[25]Johnson, W., *Helicopter Theory*, Princeton Univ. Press, Princeton, NJ, 1980, p. 942.

[26]Caradonna, F. X., Strawn, R. C., and Bridgeman, J. O., "An Experimental and Computational Study of Rotor-Vortex Interactions," *Vertica*, Vol. 12, No. 4, 1988, pp. 315–327.

[27]Srinivasan, G. R., and McCroskey, W. J., "Euler Calculations of Unsteady Interaction of Advancing Rotor with a Line Vortex," *AIAA Journal*, Vol. 31, No. 9, 1993, pp. 1659–1666.